Applied Thermal Engineering 167 (2020) 114700

Contents lists available at ScienceDirect

Applied Thermal Engineering

journal homepage: www.elsevier.com/locate/apthermeng

Investigation of 3D manifold architecture heat sinks in air-cooled condensers

Chirag R. Kharangate[a,*], Will Libeer[b], James Palko[c], Hyoungsoon Lee[d], Jessica Shi[e], Mehdi Asheghi[b], Kenneth E. Goodson[b]

[a] Mechanical and Aerospace Engineering Department, Case Western Reserve University, Cleveland, OH, USA
[b] Mechanical Engineering Department, Stanford University, Stanford, CA, USA
[c] Mechanical Engineering Department, University of California, Merced, CA, USA
[d] School of Mechanical Engineering, Chung-Ang University, Seoul, South Korea
[e] Electric Power Research Institute, Inc., Palo Alto, CA, USA

HIGHLIGHTS

- Study explores the performance of the air-side of a traditional ACC heat sink.
- A novel 3D manifolding architecture heat sink design is implemented.
- Various manifold designs offered improved COP over traditional ACC fins.
- Results show 3D manifolds fins are a good alternative for EVAPCO ACC systems.

ARTICLE INFO

Keywords:
Air-cooled condensers
3D manifold
COP
Heat sinks
Optimization

ABSTRACT

Power plants account for a high rate of freshwater utilization in the United States. Use of air-cooled condensers (ACC) can significantly reduce or completely eliminate freshwater withdrawals for steam-electric plants but suffer from low heat transfer of single-phase air flow. In the current study, we experimentally and computationally investigate the thermal-hydraulic performance of the air-side of a traditional ACC heat sink (EVAPCO fins) and conduct an extensive comparative CFD study of a novel 3D manifolding architecture heat sink design. A parametric investigation was performed on the 3D manifold heat sinks with fin height ranging from 7.3 to 15.3 mm, three fin densities with fin pitch ranging from 1 to 3 mm, and fin angles between 0° and 45°. It is concluded that there is not a single optimal design over the range of flow rates/heat flux, and the heat sink performances are a strong function of the target operating heat flux. Overall, various manifold designs were able to offer improved COP over EVAPCO fins that covered a large range of the operating heat fluxes. Manifold designs also require less fin array material, making them a good alternative for EVAPCO ACC systems if it is desired to increase the heat flux by 3 times for the existing EVAPCO units.

1. Introduction

Water is very important to the energy sector with significant usage seen in nuclear power, natural gas steam generation, biomass generation, and hydropower generation. During power generation, 41% of the nation's freshwater withdrawals and 3% of nations freshwater consumption happen in steam-electric power plants [1]. An important component to these units which sees highest water utilization is the condenser, which relies on either once-through cooling, recirculating wet-cooling towers, or air-cooling to condense the steam exiting the turbine. Between these condensers, it is well-known that air-cooled condensers (ACC) can significantly reduce or completely eliminate freshwater withdrawals for steam-electric plants. However, due to performance degradation on hot days (up to a 10% power production penalty) and higher capital expenditures, their market penetration has been limited to only 1% [2]. Fig. 1(a) and (b) show a photograph and a schematic, respectively, of an ACC designed by Evapco, Inc., which is a major manufacturer of various heat exchanger systems [3]. In this design, the condenser consists of a massive A-tent structure with steam in the top pipe, 9–15 m long condenser section across the inclined walls of the A-tent, and condensed water collected in the bottom pipes [4,5]. A typical A-tent has an apex angle of 60°. The condenser section consists

* Corresponding author.
E-mail address: chirag.kharangate@case.edu (C.R. Kharangate).
URL: http://engineering.case.edu/emae/Faculty/Chirag_Kharangate (C.R. Kharangate).

https://doi.org/10.1016/j.applthermaleng.2019.114700
Received 15 July 2019; Received in revised form 18 October 2019; Accepted 17 November 2019
Available online 19 November 2019

Nomenclature

C_p	specific heat
COP	coefficient of performance
g	gravity
H	height
H_{fin}	height of the fin
H_{ch}	height fins in the channel
H_{tot}	*total* height of the channel
h	overall heat transfer coefficient; height
k	conductivity
L_{tot}	total length of the channel
p	fin pitch
P	pressure
ΔP	pressure drop
$\dot{q}$	heat transfer rate
q''	wall heat flux
Q	volumetric flow rate
Re	Reynolds number
T	temperature
T_f	fluid temperature
T_b	temperature of fin base
u	velocity of fluid
V	velocity
W_{ch}	width of the channel
W_{tot}	total width of the channel
$x1$	fins with $p = 3$ mm
$x2$	fins with $p = 1.5$ mm
$x3$	fins with $p = 1$ mm

Greek symbols

ε	effectiveness of heat sink
θ_{fin}	fin angle
ρ	density
μ	dynamic viscosity

Subscripts

avg	average
b	base
f	fluid; fin
fine	finest mesh size investigated
in	inlet to heated portion of channel
max	maximum
out	outlet to heated portion of channel

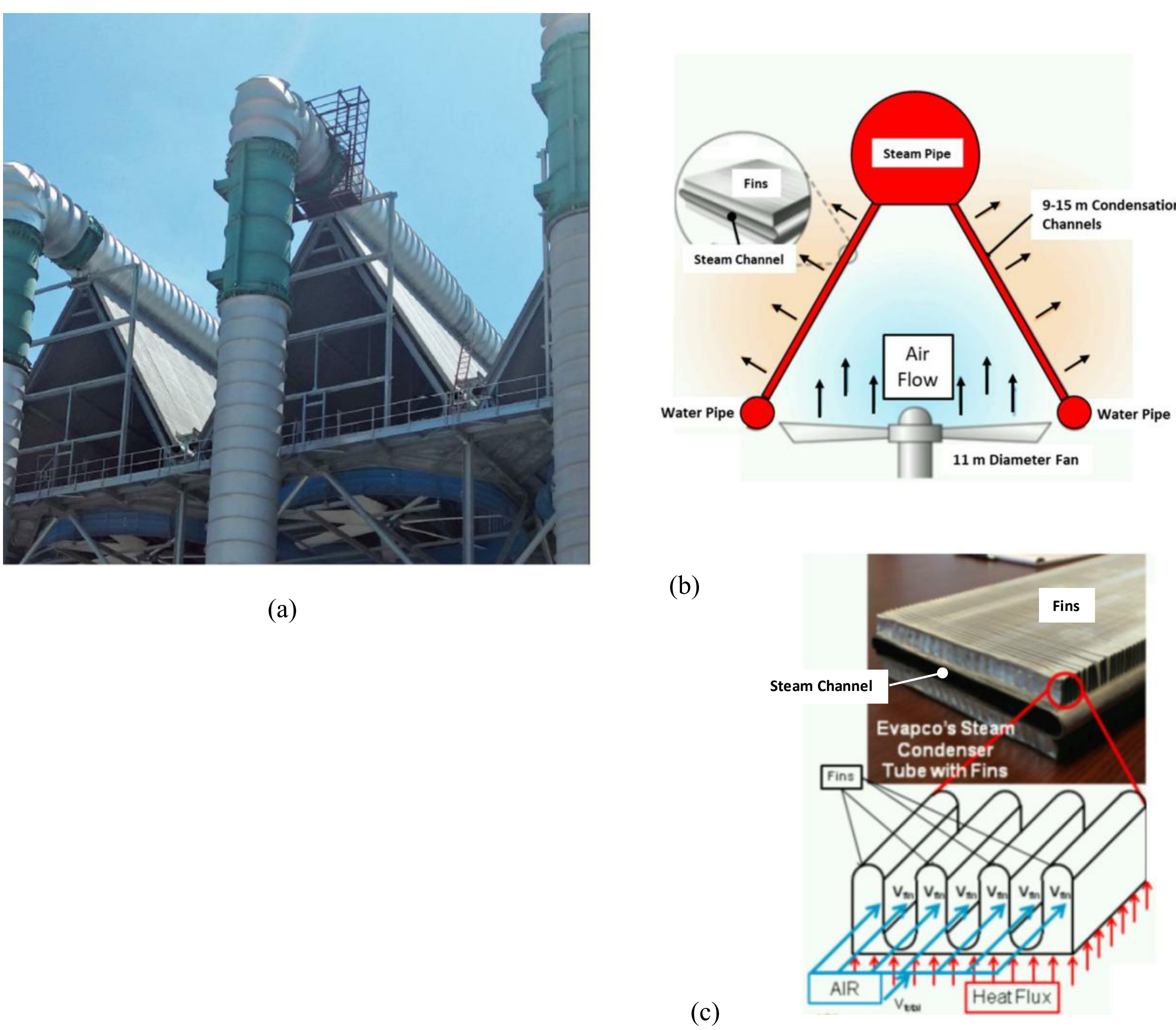

Fig. 1. (a) Photograph of EVAPCO dry-cooling tower. (b) Schematic of EVAPCO air-cooled condenser (ACC) system. (c) Section of a steam condenser tube used in ACC [3–5].

of steam channels surrounded by the aluminum folded-fin assembly as shown in Fig. 1(c). Airflow is generated using large 11 m diameter fans at the bottom of the tents. To achieve good air-side heat exchange, relatively long (~2 m) finned passages are needed due to the low heat transfer of single-phase air flow. Even after this, ACC air-side heat transfer coefficients are generally low (~35 W/m^2 K) [6]. Therefore, there is a need to improve air-side heat exchange that will reduce total thermal resistance and translate into reductions in steam condensation temperatures.

In the last two decades, there have been significant advancements made in efficiencies of ACC. This work has focused on the total ACC system designs with improvements in performance by reducing the effects of adverse winds. Meyer [7] numerically investigated the effects of adding a walkway at the edge of the fan platform flow or removing of the peripheral fan inlet section. Hotchkiss et al. [8] studied the effect of inflow losses related to the off axis inflow conditions. Bredell et al. [9] investigated the inlet flow distortion effect on fan flow rates and its impact on ACC performance. Liu et al. [10] numerically investigated the effects of different wind speed and wind direction on understanding the hot air recirculation in ACCs. Zhang et al. [11] added windbreak mesh to increase volumetric effectiveness of the inner fans, showing how a rectangular-mesh configuration negates the effects of wind. Liao et al. [12] added a triangularly shaped heat exchanger bundle around a cooling tower and showed that it improves performance in regions with strong prevailing winds. Lu et al. [13] investigated the effects of tri-blade-like windbreak wall in conventional large natural draft dry cooling towers and showed an improvement in performance. Kong et al. [14] investigated circular arranged ACCs to show a reduction in hot plume recirculation and reverse flows. In another study, Kong et al. [15] compared performances of five different windbreakers and showed how it can be used under adverse wind conditions to maintain good performance. Liu et al. [16] showed how a tower inlet cover improves the performance in natural draft dry cooling towers under crosswind conditions. Goodarzi and Ramezanpour [17] testes various cooling tower shapes and suggested that cooling towers with elliptical cross section improves cooling efficiency in comparison to the traditional circular cross-section. In a recent study. Kong et al. [18] proposed a horizontally in line arranged fin tube bundles inside the dry cooling tower and vertically in line configured bundles outside the tower and numerically investigated it to show improvement in performance.

While a lot of focus has been placed on the system design and understanding the impacts of ambient conditions like wind, the air-side fins configurations have been maintained the same as shown in Fig. 1(c) in most of the current ACC designs. Air-cooling has many advantages in comparison to liquid cooling in terms of reliability, cost, and operation. However, the heat transfer rates when utilizing air-cooling are low which limit their thermal performance and reduces the ACC performance. A few common ways that can be used to increase the thermal performance on the air-side are to enhance the surface area of heat transfer, enhance local heat transfer coefficients by surface enhancements, and increase flow rates of air. Many of these enhancement techniques when increasing the heat transfer rates also increase the pressure drops, and therefore, the pumping power requirements of the air-cooled system. What this means to ACC systems is that higher power fans are needed in the A-tents which impact the capital expenditure and operating cost. In a recent study, Bustamante et al. [6] investigated how some emerging heat transfer enhancement techniques can be used to achieve high-efficiency levels approaching that of a water-cooled power plant in air-cooled systems. Some of the ways include conventional fin enhancement techniques [19], use of vortex generators [20], jet impingement configurations [21,22], and use of external flows like electrohydrodynamics (EHD) [23] and ultrasound [24]. Another way to achieving high heat transfer while limiting the pressure drop is the use of fluid manifolding architectures that have been utilized a lot recently in liquid-cooling systems. Past few decades have seen researchers designing manifolding architectures in different ways, which includes the tree-like or fractal-based networks [25–27] or through the more practical manifolding architecture microchannels [28]. A 3D manifold design that will be used in this study is an adaptation of the original concept by Ohadi et al. [29]. Fig. 2 shows a section of the air side of the heat sink and illustrates how the flow moves through the channel: (1) Cold air travels into the "converging" manifold and distributes from entrance to the end of the manifold to the fin array underneath (blue arrows). (2) Air travels down inside the fin array, 90° down. (3) As air moves laterally through the dense fins (blue/red arrows), it heats up as it moves along the base of the fin array. The air sees a large fin surface area while only traveling short distances within the fin channels. (4) Then, it makes a 90° turn upwards, out of the fin array (red arrows). (5) The heated air exits out of the "diverging" manifold section (red arrows). Such 3-dimensional fluidic routing leads to lower flow velocities experienced by the fins that reduce the pressure drop, and the developing thermal-hydraulic nature of the flow increases the heat transfer coefficients leading to higher heat exchanger performances. The main advantage of this design to air-cooling in our system is that the heat transfer enhancement can be archived without the need for microchannels which have significant pumping requirements. In recent work, Arie et al. [30] tested dry heat exchangers that show up to 25% increase in heat transfer density in comparison to a similar COP traditional heat exchanger design.

In the current study, we will first experimentally investigate the

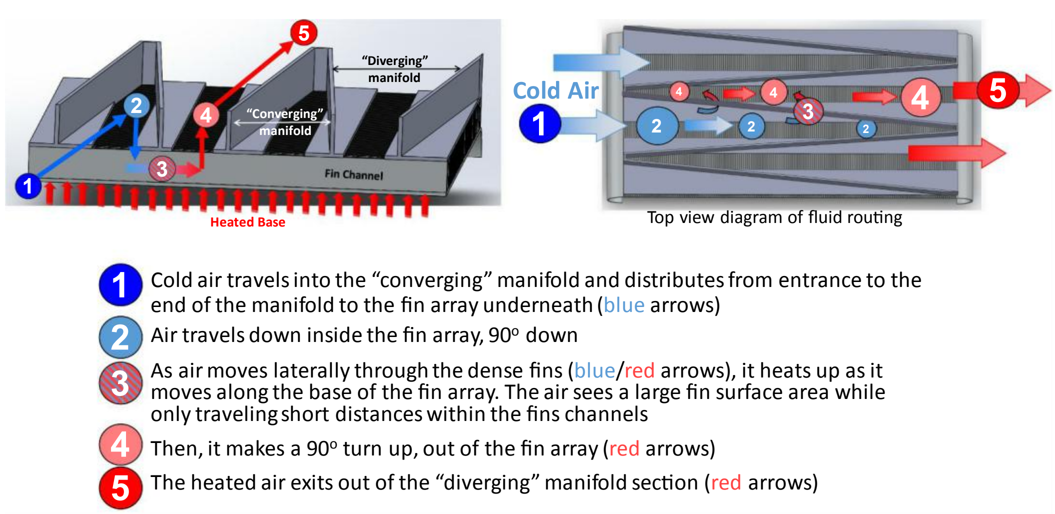

Fig. 2. 3D manifold architecture designed to fit in the EVAPCO fins configuration.

thermal-hydraulic performance of the air-side of a traditional Evapco ACC. The traditional fins investigated in this study were provided by Evapco, Inc. and are straight aluminum fins with height of 19 mm, thickness of 0.3 mm, and pitch of 3 mm in a total flow volume that has a length of 203.2 mm, height of 20 mm, and width of 101.6 mm as shown in Fig. 3. These traditional ACC fins will be labeled as EVAPCO fins throughout this study. The experimental data will be validated by comparing them with reduced order modeling and computational fluid dynamics (CFD) simulation results.

Then, we propose a novel 3D manifolding architecture heat sink design, and conduct systematic CFD modeling in an attempt to improve the performance metrics such as ACC size, footprint, weight, heat transfer characteristic and pressure drop, compared to the Evapco ACC heat sink design. The proposed 3D manifolding heat sinks take up the same volume total as the traditional design with three fin heights, h = 7.3, 11.3, and 15.3 mm, three fin pitches, p = 1, 1.5 and 3 mm, and three fin angles, θ = 15, 30 and 45°, will be investigated computationally to perform a thorough design optimization. The schematics of the manifold architecture depicting the parameters investigated for fin heights, fin densities, and fin angles have been shown in Fig. 4(a), (b), and (c), respectively. CFD investigation was also performed to see if there are better performing fin densities of the EVAPCO fins with three fin pitches, p = 1, 1.5 and 3 mm. CFD results will be used to estimate the coefficient of performance (COP) of the 3D manifold fins and compare with the traditional fin designs. Optimal designs will be recommended for ranges of working heat fluxes of ACC.

2. Experiment

To develop a baseline for this study, the EVAPCO fins were tested experimentally to study the air-side thermal hydraulic performance. The experiments were conducted by building a flow channel as shown in Fig. 5(a) with air flowing into an inlet plenum for hydrodynamic flow development, followed by the heated section with straight fins where heat transfer and pressure drops are measured, and finally through an exit plenum before exiting the flow channel. The heated section of the channel used the straight fins with 0.3 mm thickness, 19 mm height, and 3 mm width on a channel with a total length of 203.2 mm and a total width of 101.6 mm as shown in Fig. 5(b). The back side of the fin base was instrumented with 8 film-heaters, all connected in parallel electrically, to simulate a uniform heat flux boundary condition as shown in Fig. 5(c). T-type thermocouples were placed at three locations along the centerline of the heated section to make wall temperature measurements. Pressure drop was measured utilizing a differential pressure gauge across the heated portion of the channel. Flow velocities were measured at two locations in the test channel, one the inlet plenum and another the exit plenum. The complete experiment assembly is shown in Fig. 5(d). The operating conditions for the experimental study are as follows: Air inlet temperature of $T_{f,in}$ = 19.3–20.3 °C, inlet velocity of 3.5–6 m/s, and average wall heat flux of q'' = 1.9–10.2 kW/m^2.

3. Computational model

In this study, CFD simulations will be performed on EVAPCO fins and various 3D manifold architecture designs. Fig. 6(a) shows the computational domain used in the simulations for the EVAPCO fins, which indicates the unit-cell width and the total length of the flow channel. Fig. 6(b) shows the computational domain used in the simulations for the 3D manifold heat sink, which indicates the unit-cell width of the manifold and the total length of the flow channel. In both cases, a velocity inlet (ranging from 0.25 to 6 m/s) and a temperature inlet condition (T_{in} = 313.15 K) were used as the inlet boundary conditions, and a pressure outlet condition was applied as the outlet boundary condition. For the EVAPCO fins CFD simulations, a constant heat flux boundary condition (q'' = 1800–10200 W/m^2) is applied when the results were compared to the experimental data. For the rest of the comparative study between the EVAPCO and proposed novel 3D manifold, a constant temperature boundary condition is used on the bottom wall to simulate the constant-temperature condensing water vapor (T_{wall} = 353.15 K). The symmetry boundary condition is used on the side walls of both the domains. In both cases, the flow length is extended at the exit of the domain to minimize any end effects due to the outlet boundary conditions. The material for both configurations is aluminum with conductivity, k = 202.4 W/mK. Commercial CFD software, ANSYS FLUENT 17.0, was used to compute the continuity, momentum, and energy conservation equations of the simulation domains. The constitutive equations are as follows: continuity,

$$\nabla \cdot u = 0, \tag{1}$$

conservation of momentum,

$$\rho\,(u \cdot \nabla\, u) = -\nabla P + \mu\, \nabla^2 u + \rho\, g, \tag{2}$$

and conservation of energy,

$$\rho\, Cp\ (u \cdot \nabla\, T) = \nabla\,(k\, \nabla T) + \mu\, \Phi. \tag{3}$$

EVAPCO Geometry

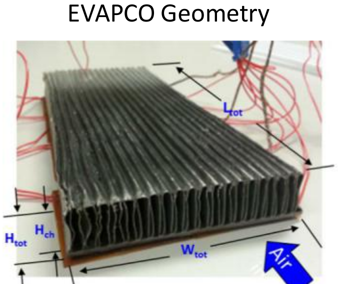

Dimensions (mm)	EVAPCO	3D Manifold
Total height	20	20
Channel height	19	19
Base thickness	1	1
Channel length	203.2	203.2
Total width	101.6	101.6

3D Manifold Geometry

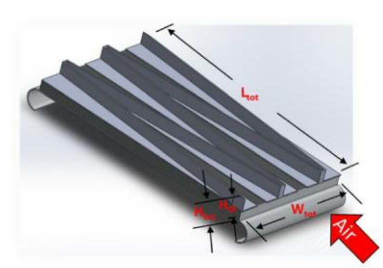

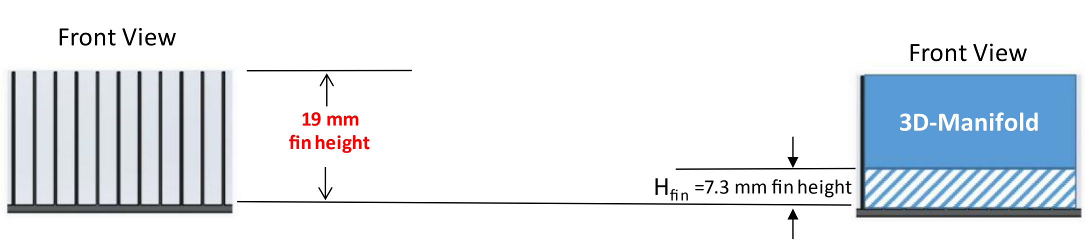

Fig. 3. A comparison between EVAPCO fins heat sink design and a configuration with 3D manifold architecture heat sink design.

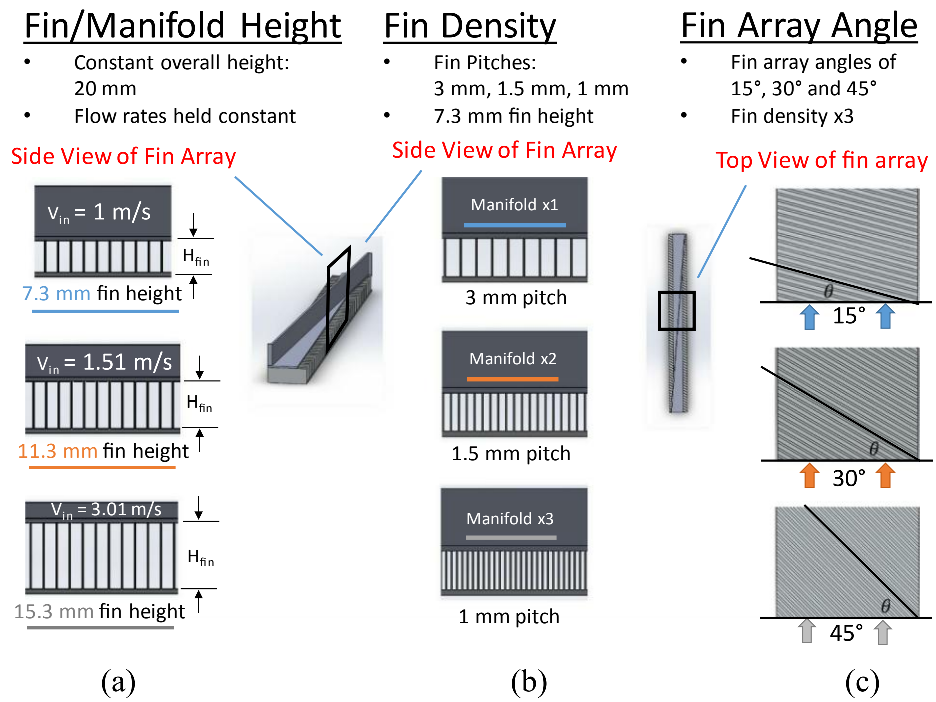

Fig. 4. (a) Side view of 3D manifold fin array showing three heights of manifold fins. (b) Side view of 3D manifold fin array showing three pitches of manifold fins. (c) Top view of 3D manifold fin array showing three angles of manifold fins.

A pressure-based solver was used for these simulations. Pressure-velocity coupling was achieved using the Semi-Implicit Method for Pressure-Linked Equations (SIMPLE) algorithm. Gradient discretization was done using the least-squares cell-based scheme, pressure discretization wad done using the second order scheme, momentum, and energy discretization was done using the second upwind scheme. For all test cases investigated in this study, $Re \leq 2000$, so the laminar viscous model was selected. Test cases at the high end of the Reynolds number were verified by running the k-ε turbulence model and the results were compared with the laminar viscous model. Simulations show that the laminar viscous model was sufficient for all the test cases. ANSYS Meshing was utilized to generate a mesh with conformal hexahedral elements. Mesh independence was verified before selecting the final mesh. A detailed discussion on the mesh independence study is included in Appendix A. Because different computational domains are being investigated, different mesh sizes were necessary for each

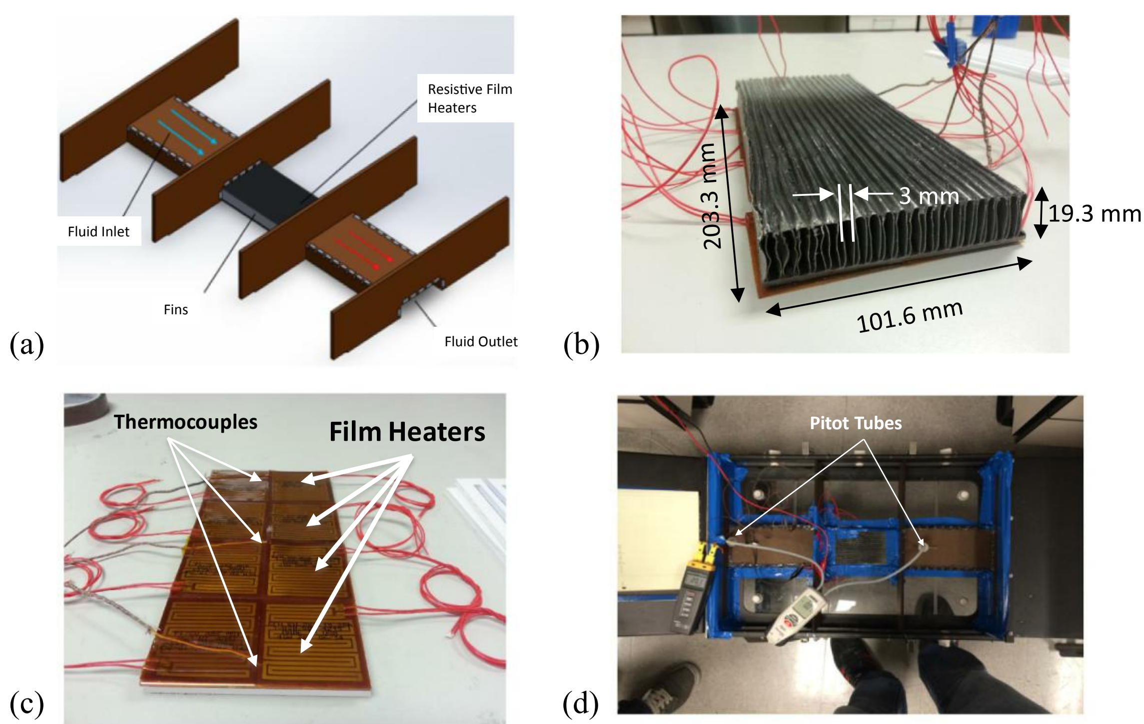

Fig. 5. (a) CAD schematic of the wind tunnel experiment. (b) EVAPCO folded fins design with dimensions. (c) Heater design showing 8 film heaters spread across the wall to achieve uniform heat flux and thermocouples assembly with thermocouples placed a three locations along the centreline. (d) Photo of the experimental setup.

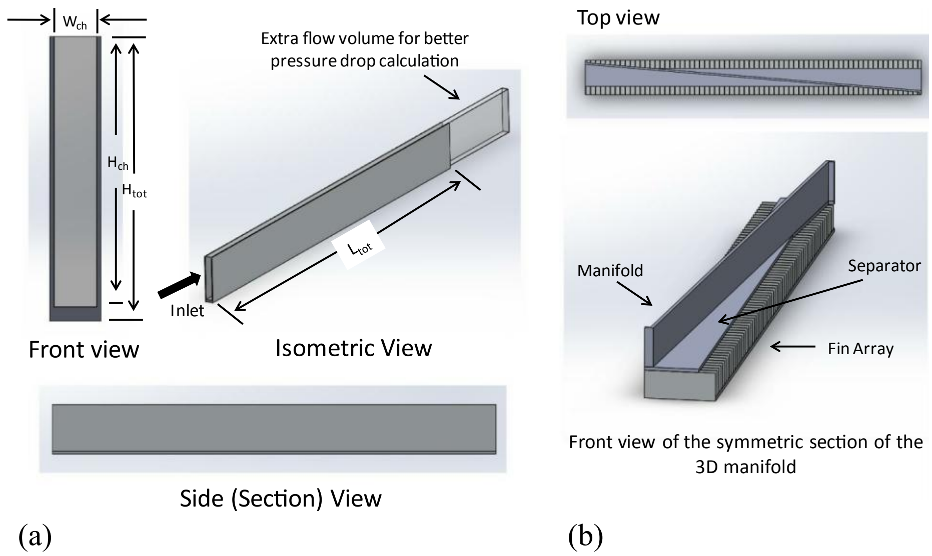

Fig. 6. (a) Simulation domain for EVAPCO fins. (b) Simulation domain for 3D manifold design heat sink.

Table 1
Heat Transfer and pressure drop correlations for reduced-order model [30].

Heat Transfer	Pressure Drop
$Nu_{\Delta z}=8.235(1-1.883\beta+3.767\beta^2-5.814\beta^3+5.361\beta^4-2.0\beta^5)$ $\beta=H_{ch}/W_{ch}$	$\Delta P_{\Delta z}=\frac{2L_{ch}}{D_h}fG^2v_{air}$ where f is the fanning friction factor $Re<2000$ $fRe=24(1-1.3553\beta+1.9467\beta^2-1.7012\beta^3-0.9564\beta^4-0.2537\beta^5)$ $2000<Re<20000$ $f=0.079Re^{-0.25}$ $Re>20000$ $f=0.046Re^{-0.2}$

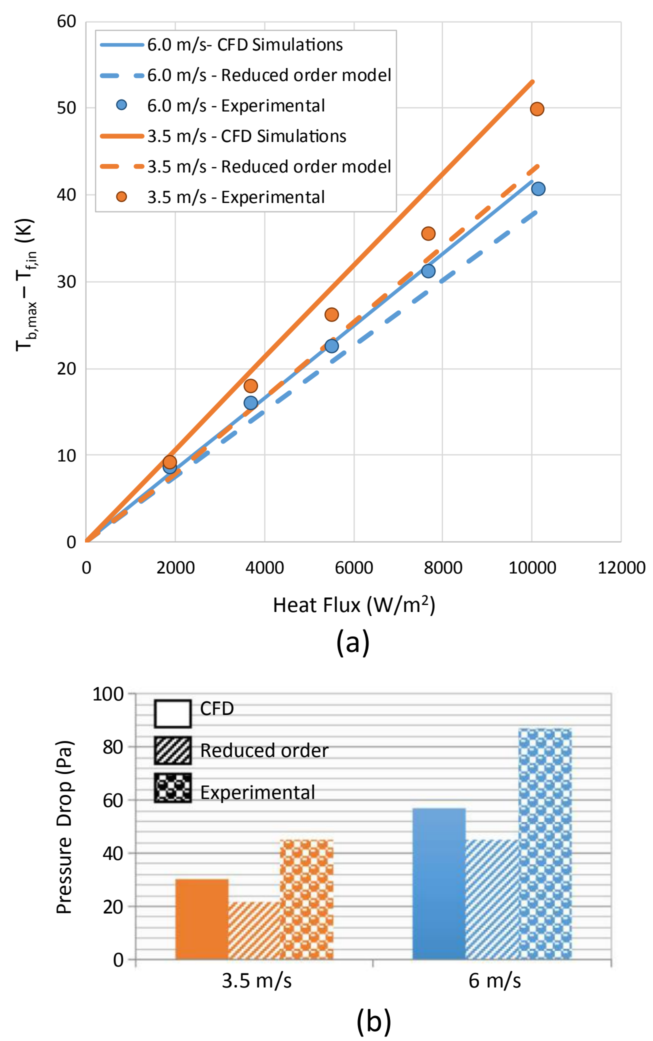

Fig. 7. EVAPCO fin design data based on CFD, reduced order model and experiments: (a) temperature difference vs. base heat flux, and (b) pressure drop vs. inlet velocity.

domain. In each case, the finest mesh for which the pressure drops reached asymptotic values was used to calculate the results presented in this study. CFD simulations used the following boundary conditions: inlet temperature of $T_{f,in}=40$ °C, wall temperature of $T_b=80$ °C, and inlet velocity based on the total cross-sectional area of the channel of 0.25–6.0 m/s. The inlet velocity for the manifold channel was estimated based on the mass flow rate in the full cross-section of the channel (20 mm in height) being restricted to the manifold channel cross-section (height of the manifold).

4. Results and discussion

To validate the CFD simulations for the EVAPCO fins, the experimental data for the wall temperature and the pressure drop across the EVAPCO fins are compared with results from the reduced order model and CFD simulations. For reduced order modeling, Nusselt number and pressure drop were calculated based on correlations for rectangular ducts provided in Shah and London [31]. Table 1 shows the correlations used to calculate the two parameters at each axial location. In the reduced order model, the flow channel is sub-divided into Δz increments and the heat transfer coefficient and pressure drop for each increment is calculated starting from the upstream section to the downstream section of the fins. On analysis, it was observed that 1000 subdivisions were enough for a converged solution for both the heat transfer and pressure drop variation. At each axial location, the wall temperatures were computed by using a simple resistance model between the air temperature and solid aluminum fins. A detailed description of this approach can be found in Jung et al. [32].

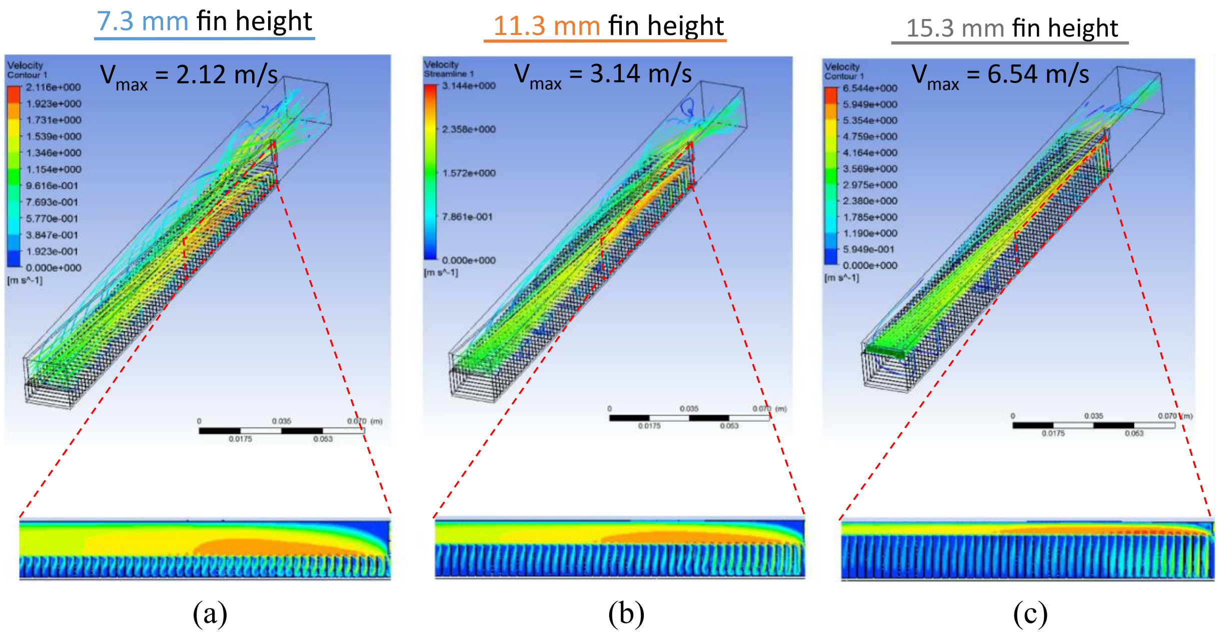

Fig. 8. Velocity contours obtained with a fixed flow rate of 2.19×10^{-4} m^3/s for (a) fin height of 7.3 mm, (b) fin height of 11.3 mm, and (d) fin height of 15.3 mm. [Color scales not the same for the three parts, corresponding maximum velocities stated.]

Fig. 7(a) compares the temperature difference between the maximum temperature of the base and the inlet air temperature with the heat flux. We can see that there is a reasonable agreement between the experimental data, reduced order model and CFD simulations. The CFD simulations do a better job at higher velocity of 6 m/s in comparison to a velocity of 3.5 m/s, which can be attributed to the lower heat losses in the higher flow rate test case. However, some variation from the experiment is attributed to the irregularity in these EVAPCO fins that the model and simulations cannot capture. The irregularity in fin structure leads to the flow being more turbulent in the experiment, that will give higher pressure drops and lower wall temperatures as observed. Fig. 7(b) compares the pressure drop across the fins. Here, we can see that the experimental data is underpredicted in both cases. A reason for this behavior is the irregularity that we can see in the EVAPCO fins shown in Fig. 5(b) that the model and simulations cannot capture.

To access the thermal-hydraulic performance of the different heat sink designs, a COP was determined, which is expressed as,

$$COP = \frac{\dot{q}}{Q\,\Delta P}, \tag{4}$$

where $\dot{q}$ is the rate of heat transfer, Q is the volume flow rate, and ΔP is the pressure drop across the fins. The COP gives us a measure of the ratio of heat transfer to the work done across the fins. While keeping thermal-fluidic boundary conditions and total volume of the heat sinks constant, the three main parameters of interest, which will be discussed in this study, are the input parameter, flow rate, and output parameters, heat transfer rate and pressure drop. COP gives a good measure of the combined effects of these parameters and was therefore, selected as the choice for performance evaluation. Another parameter that will be used to assess the performance of the heat sink is the effectiveness, which is expressed as,

$$\varepsilon = \frac{(T_{f,out} - T_{f,in})}{(T_{b,avg} - T_{f,in})}, \tag{5}$$

where $T_{f,out}$ is the outlet air temperature, $T_{f,in}$ is the inlet air temperature, and $T_{b,avg}$ is the average temperature of the fin base. The effectiveness is a measure of the utilization of the fluid for heat transfer. To perform optimization on the manifold design, we change three manifold heat sink parameters, namely, fin height (h = 7.3, 11.3 and 15.3 mm), fin density (p = 3 mm (Case $x1$), p = 1.5 mm (Case $x2$) and p = 1 mm (Case $x3$)) and fin angle (θ_{fin} = 0°, 15°, 30° and 45°). Results from each of these parametric studies will be discussed in detail in this section and used to down-select fin configurations.

We start with the first parameter, fin height. While the total height of the channel is kept constant at 20 mm, the height of the fins is varied from 7.3–15.3 mm. Changes in fin height also change the height of the manifold section because the total cross-section area is kept constant. Fig. 8(a)-(c) compares the velocity contours obtained for the three cases with fin heights h = 7.3, 11.3 and 15.3 mm where the flow rate Q was held constant at 2.19×10^{-4} m^3/s. The velocity contours show air moving into the manifold channel, turning down into the fin channels

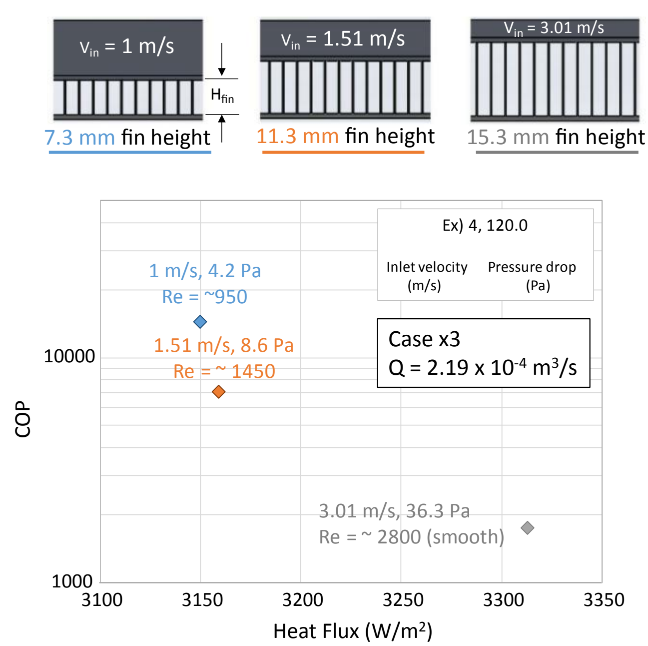

Fig. 9. COP vs. heat flux for three fin heights in straight (θ_{fin} = 0°) 3D manifold design with fin pitch, p = 3 mm (Case ×1) and a fixed flow rate, $Q = 2.19 \times 10^{-4}$ m^3/s.

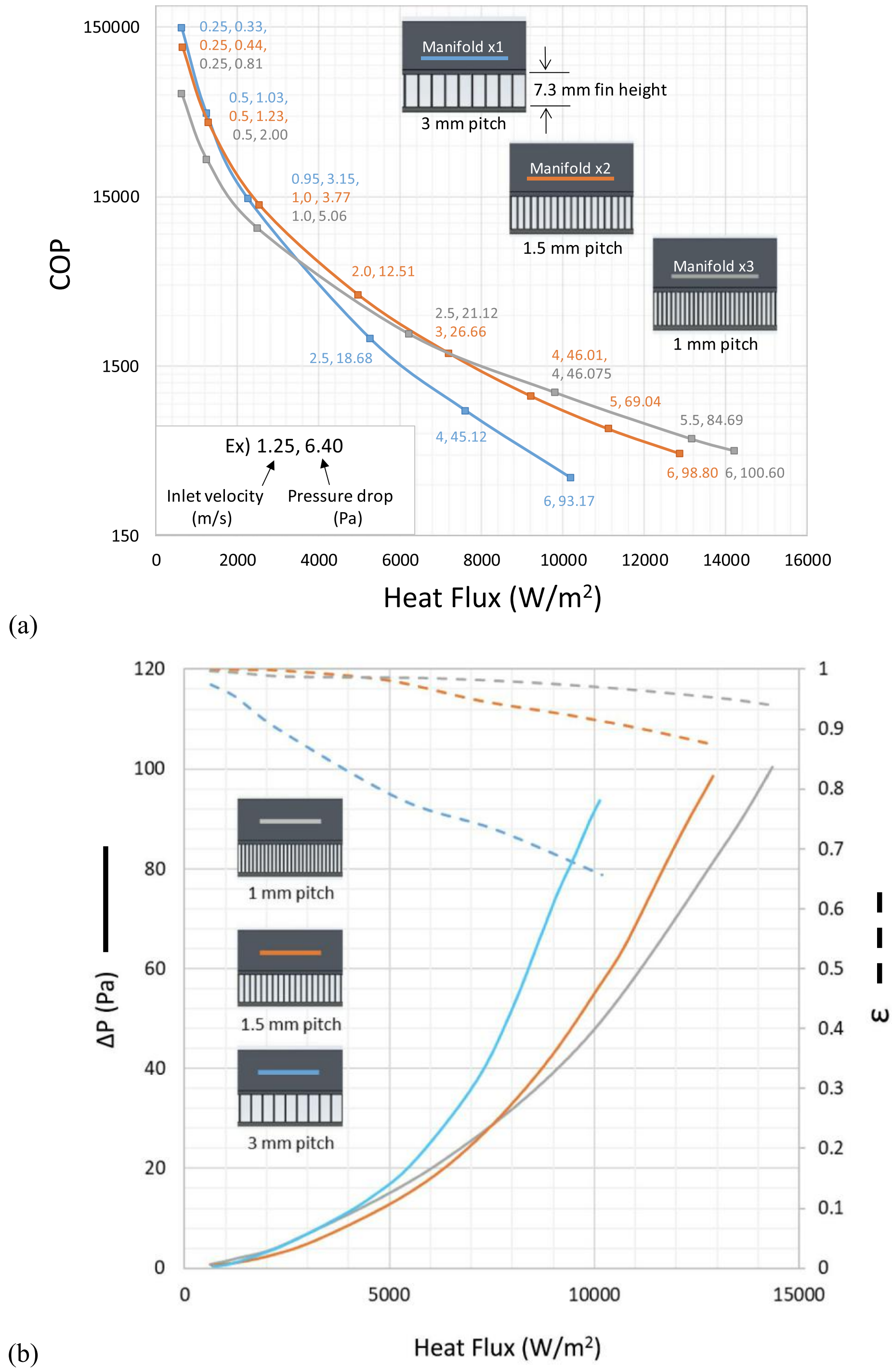

Fig. 10. For three fin pitches of the 3D manifold, (a) COP vs. heat flux and (b) pressure drop and effectiveness vs. heat flux.

section, crossing the fin section, and moving up into the manifold section before exiting the heat sink. As can be seen in Fig. 8(a), the transition of air to the fin channels is seen to be smoother for the smallest height of the fin. As we see in Fig. 8(b) and (c), a larger height of the fin shows extreme velocity gradients in the exit region. This behavior is bound to impact the pressure drops across the channels which potentially will reduce COP. Fig. 9 shows the variation of COP vs. base heat flux for the three fin heights. The plot shows that fin heights of 7.3 mm and 11.3 mm have similar heat fluxes, however, the COP of 7.3 mm fin is almost two times that of 11.3 mm fin which is related to the increase in pressure drop in these channels. As expected, there is a very sharp reduction in COP performance when we go to the fin height of 15.3 mm. We can conclude from this that the 7.3 mm fins are optimal to be further investigated. For all results discussed after this, we will only use fins with a height of 7.3 mm.

The second parameter we investigate is the fin density and this was done by varying the pitch of the fins: $p = 3$ mm (Case *x1*), $p = 1.5$ mm (Case *x2*) and $p = 1$ mm (Case *x3*). Fig. 10(a) compares the results obtained for COP vs. heat flux for inlet flow velocities 0.25–6 m/s. We can see that a clear trend emerges where low fin density is optimal for low velocities and high fin density is optimal for high velocities. Each fin density has a region of optimal performance: *x1* for $q'' \le 1200$ W/m^2, *x2* for $1200 \le q'' \le 5500$ W/m^2, and *x3* for $q'' \ge 7200$ W/m^2. This trend can be explained by examining the relationship between fin

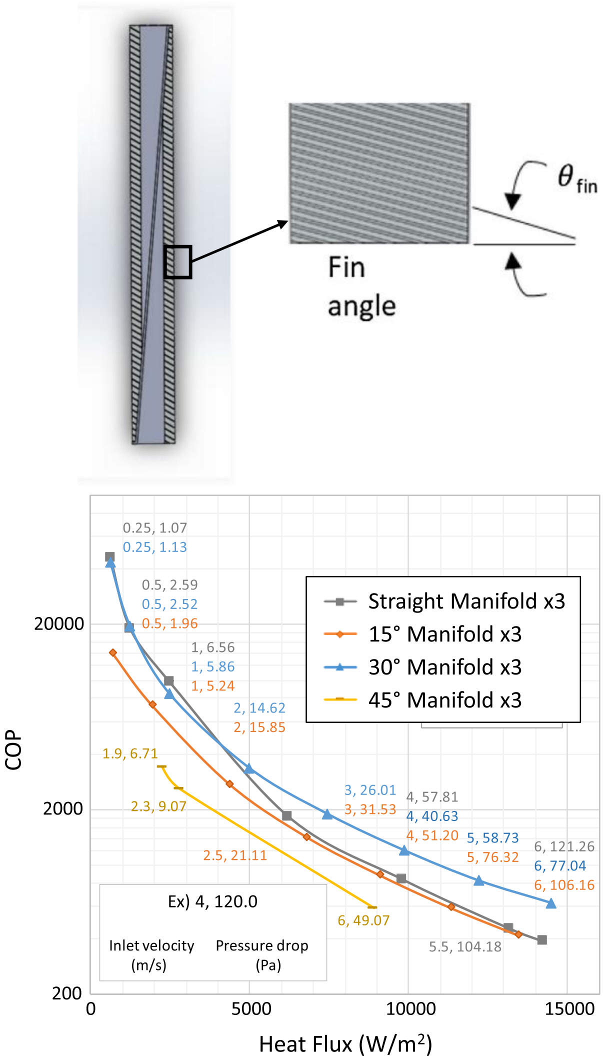

Fig. 11. COP vs. heat flux for four fin angles (θ_{fin} = 0°, 15°, 30° and 45°) in the 3D manifold with fin pitch fixed at 1 mm (Case *x*3). Inlet velocities varied from 0.25 to 6 m/s for all the fin angles.

effectiveness and heat flux. Fig. 10(b) compares the pressure drops and fin effectiveness for the three fin densities. Due to the increase in surface area, the effectiveness of a given heat flux increases with fin density. In particular, the effectiveness decreases much more rapidly for the *x1* case than for the *x2* or *x3* cases. The *x1* case needs higher velocities to reach a given heat flux, and thus, the pressure drop for a given heat flux is larger than for the *x2* or *x3* cases. The rapidly decreasing effectiveness values and increasing pressure drop values for the low fin density cases result in better performance for the higher density fins at higher heat fluxes.

The third parameter we investigate is the fin angle. The top views of the manifold channel describing how the fin angles θ are varied from 0° to 45° in 15° intervals are depicted in Fig. 4(c). Fig. 11 compares the results obtained for COP vs. heat flux for inlet flow velocities 0.25–6 m/s and different fin angles of the manifold. The straight manifold *x3* was the highest performing overall at low heat fluxes but is overtaken by 30° array due to the straight array's higher pressure drops at high velocities due to the sharp turn in air flow, and more rapidly decreasing effectiveness. Angling the fins reduces pressure drop but also causes some sections neat the inlet and outlet to not get enough air flow reducing heat transfer. 30° fins were seen to give a good compromise between these two competing effects, and therefore, this configuration provided the best performance for higher heat fluxes. The 45° case suffers from poor performance despite the lowest pressure drops which are a function of the easier flow transition through the manifold in comparison to other angles. Overall, we can say that straight fins case performs well for low heat fluxes, and 30° case performs better at high heat fluxes.

To get a full view of these optimization studies, we now compare the performances for 8 different cases that we select based on the earlier results: three EVAPCO fins with p = 3 mm (EVAPCO *x1*), p = 1.5 mm (EVAPCO *x2*) and p = 1 mm (EVAPCO *x3*), three straight manifold configurations with p = 3 mm (Manifold *x1*), p = 1.5 mm (Manifold *x2*) and p = 1 mm (Manifold *x3*), and 30° angled manifold fins with p = 1 mm (30° Manifold *x3*). Fig. 12(a) shows the COP vs. heat flux for these eight cases. Table 2 shows the important input and output parameters from CFD simulations for some selected test configurations. We can see that there is no one clear design or configuration that performs best for the whole range of heat fluxes. The first region of interest contains high COP values with corresponding lower heat flux values obtained at relatively low flow rates and is shown in Fig. 12(b). At the lowest flow rates, the straight manifolds outperform EVAPCO *x1* unit. The straight manifold *x1* is the highest performing for $q'' \leq$ 1500 W/m^2. Above that heat flux, straight manifold *x2* shows the best performance for 1500 W/m^2 < $q'' \leq$ 5500 W/m^2. The second region of interest contains moderate COP values. As seen in Fig. 12(a), here geometry performance curves start to overlap, showing many different high performing cases depending on heat flux, with EVAPCO *x1* unit maintaining very close to the highest or the highest COPs for most of the range of 5500 W/m^2 < $q'' \leq$ 8000 W/m^2. The third region contains low COP values with corresponding higher heat flux values obtained at relatively high flow rates and is shown in Fig. 12(c). In this section of the plot, the EVAPCO *x1* unit originally has the highest COP per heat flux but is overtaken at higher flow rates by the manifolds for q'' > 8000 W/m^2. The straight manifold *x3* shows the best performance for 8000 W/m^2 < $q'' \leq$ 12000 W/m^2. At the highest flow rates with q'' > 12000 W/m^2, the 30° manifold *x3* outperforms the straight manifold *x3* unit. These results follow the trend seen in the earlier fin density trials where high fin densities are suitable for higher heat fluxes and low fin densities for lower heat fluxes. Another important parameter that impacts the cost and should be discussed is the material utilization in each of these cases with EVAPCO and manifold fins. Fig. 12(d) compares the percentage volume occupied by aluminum to estimate the amount of material needed in each design. It can be seen that straight manifold *x1* and straight manifold *x2* utilize lower mass of aluminum in comparison to the EVAPCO *x1* unit. As expected, higher density fins increase the material utilization. In general, moving to manifold heatsinks show there is an advantage of the lower material unitization which will reduce initial capital investment and plant footprint.

The findings of this study demonstrate that the existing design of the ACC air-side heat sinks (EVAPCO fins) performs well over a specific range of heat fluxes. However, by performing a series of optimizations, we have shown that for a large range of heat fluxes, the innovative fin array with 3D manifolding architecture can be used to replace the EVAPCO heat sink and achieve better thermal-hydraulic performance. It should be noted that optimization of the manifold design is not complete because only a select few parameter variations were investigated in this study. A future study with more fin heights, fin densities, and fin angles can be used to refine and improve the performance achieved by the manifold heat sinks. Also, as no experimental tests of the 3D manifold designs were conducted, future studies should involve the full experimental validation of the CFD simulation results obtained in this study.

5. Conclusions

In the current study, we investigated computationally the thermal-hydraulic performance of the air-side of a traditional ACC heat sink (EVAPCO fins) and developed 3D manifolding architecture heat sink

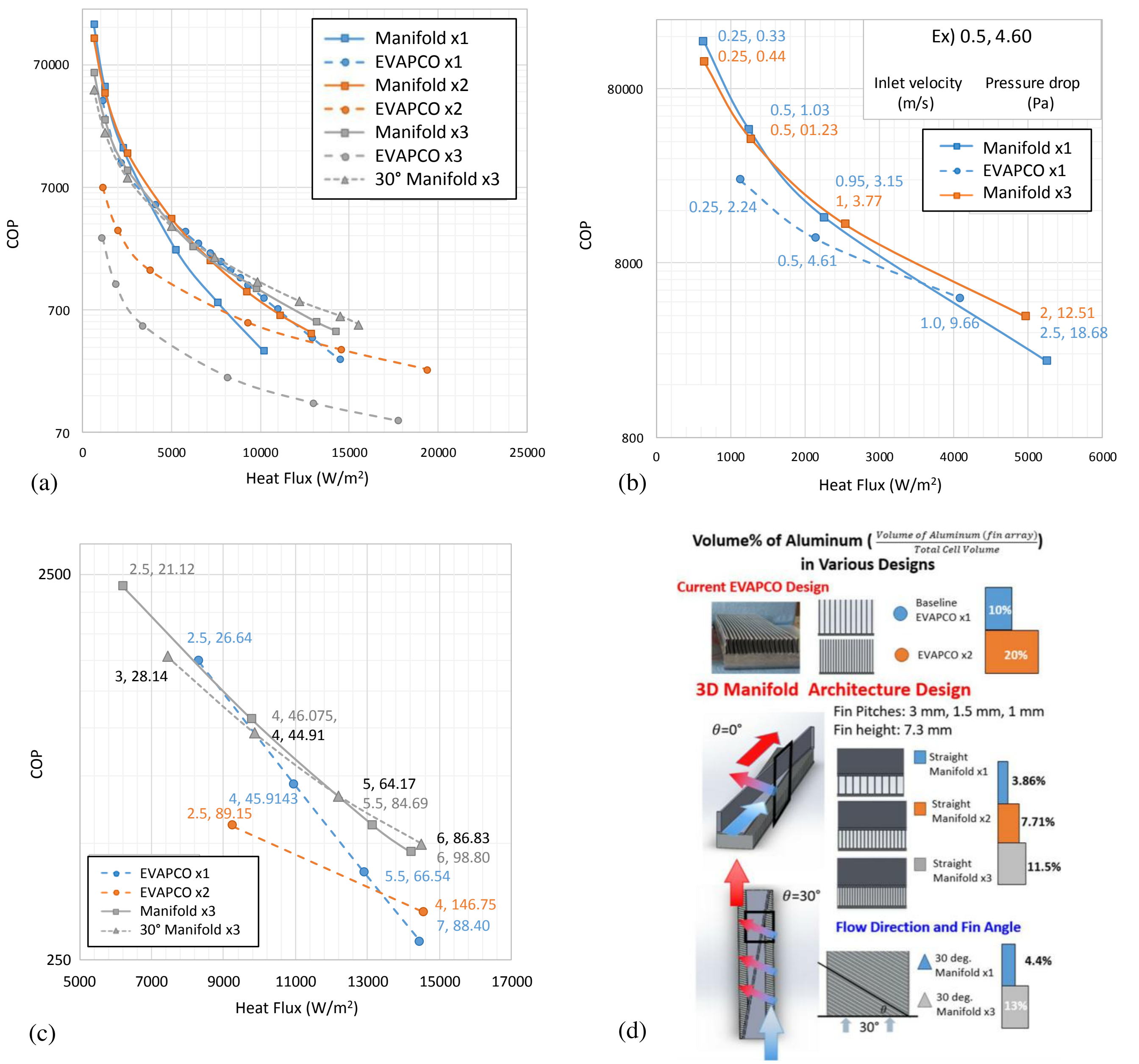

Fig. 12. (a) COP vs. heat flux for various EVAPCO and 3D manifold heat sing designs. (b) Expanded plot of COP vs. heat flux for heat fluxes up to 5250 W/m^2 ranges. (c) Expanded plot of COP vs. heat flux for heat fluxes between 5250 W/m^2 and 14500 W/m^2. (d) Comparison for volume percentage of aluminium between the heat sink designs.

designs to replace the traditional heat sinks without significantly increasing the ACC size and fan power consumption. A parametric investigation was performed to optimize the manifold design for a range of flow and thermal conditions of the condenser. Key findings from the study are as follows.

(1) EVAPCO heatsinks were tested experimentally and the data were validated with CFD simulations and reduced order modeling. While wall temperatures were predicted well, the pressure drop was underpredicted in both cases.
(2) 3D manifold architectures provide special fluidic routing that leads to lower pressure drop and higher heat transfer coefficients in comparison to traditional heat sinks. 3D manifold heat sinks were designed to have the same form factor as the EVAPCO heat sinks.
(3) The parametric investigation was performed with three fin heights between 7.3 mm and 15.3 mm, three fin densities with fin pitches 3 mm, 1.5 mm, 1 mm, and four fin angles between 0° and 45°. A fin height of 7.3 mm was seen to provide optimal COP performance. For the fin densities, we saw a clear trend where low fin density is optimal for low heat fluxes and high fin density is optimal for high heat fluxes. Between the fin angles, we saw that straight fins with 0° angle performed better for low heat fluxes and fins with 30° angle performed better for high heat fluxes.
(4) It is seen that there is not one single optimal design, and the heat sink performances are a strong function of the operating heat flux. Different fin configurations provide regions of optimal performance: Straight manifold with fin pitch of 3 mm for $q'' \le 1500$ W/m^2, straight manifold with fin pitch of 1.5 mm for $1500 < q'' \le 5500$ W/m^2, EVAPCO fins with fin pitch of 3 mm for $5500 < q'' \le 8000$ W/m^2, straight manifold with fin pitch of 1 mm for $8000 < q'' \le 12000$ W/m^2, and 30° manifold with fin pitch of 1 mm for $q'' > 12000$ W/m^2.

Table 2
Important input and output parameters from CFD simulations for selected test configurations.

Case	V_{in} (m/s)	Q (m^3/s)	T_{out} (K)	q'' (W/m^2)	$\dot{q}$(W)	ΔP (Pa)	COP	h (W/m^{2}K)	ε
Manifold *x1*	0.25	5.48E−05	352.09	635.26	2.69	0.33	149234.62	15.88	0.9735
	0.95	2.08E−04	349.16	2263.21	9.57	3.15	14599.97	56.58	0.9002
	2.5	5.48E−04	344.47	5265.15	22.27	18.68	2176.06	131.63	0.782975
	4	8.77E−04	342.42	7615.23	32.21	45.12	814.50	190.38	0.7318
	6	1.32E−03	339.43	10198.40	43.14	100.60	326.14	254.96	0.657
EVAPCO *x1*	0.25	1.28E−05	353.15	1128.56	0.69	2.24	23924.93	28.21	1
	1	5.13E−05	352.30	4091.18	2.49	9.66	5028.75	102.28	0.97865
	2.5	1.28E−04	346.72	8326.04	5.07	26.64	1484.15	208.15	0.839225
	4	2.05E−04	342.13	10986.70	6.69	45.91	710.17	274.67	0.72455
	5.5	2.82E−04	338.90	12922.60	7.87	66.54	419.21	323.07	0.64375
Manifold *x2*	0.25	5.36E−05	353.13	639.69	2.71	0.44	114703.08	63.65	0.9995
	1	2.14E−04	353.01	2545.98	10.77	3.77	13323.08	63.65	0.996425
	2	4.29E−04	352.38	4978.84	21.06	12.51	3930.69	124.47	0.98065
	4	8.57E−04	350.14	9233.28	39.06	46.01	990.63	230.83	0.9248
	5	1.07E−03	349.18	11122.80	47.05	69.04	636.24	278.07	0.9007
EVAPCO *x2*	0.25	5.70E−06	353.15	1115.13	0.34	8.47	7030.80	27.88	1
	2.5	5.70E−05	353.09	9271.18	2.82	89.15	555.57	231.78	0.9985
	4	9.12E−05	352.61	14578.10	4.44	146.75	331.69	364.45	0.986475
	5.5	1.25E−04	351.59	19417.30	5.91	205.60	229.33	485.43	0.961
Manifold *x3*	0.25	5.36E−05	353.05	625.18	2.64	0.81	60539.71	15.63	0.997475
	2.5	5.36E−04	352.55	6217.50	26.26	21.12	2322.21	155.44	0.9849
	4	8.57E−04	352.02	9806.42	41.42	46.08	1049.08	245.16	0.9718
	5.5	1.18E−03	351.17	13169.00	55.63	84.69	557.43	329.22	0.950575
EVAPCO *x3*	0.25	3.33E−06	353.15	1090.47	0.22	24.48	2719.57	27.26	1
	2.5	3.33E−05	353.15	8158.29	1.66	249.98	199.25	203.96	1
	4	5.32E−05	353.14	12976.50	2.63	405.39	122.14	324.41	0.999825
	5.5	7.32E−05	353.10	17788.50	3.61	565.74	87.26	444.71	0.9988
30°Manifold *x3*	0.25	5.36E−05	353.14	624.12	2.64	1.13	43457.48	98.16	0.999625
	2	4.28E−04	352.59	4987.85	21.10	14.62	3367.49	656.04	0.986075
	4	8.57E−04	351.80	9859.80	41.71	40.63	1197.94	1178.42	0.966325
	6	1.29E−03	350.33	14508.10	61.37	77.04	619.72	1589.58	0.929475

(5) Results show that different manifold designs offer improved COP over EVAPCO fins over a large range of operating heat fluxes while also requiring significantly less fin array materials, making them an alternative for ACC systems.

Acknowledgment

The research reported in this work was supported, in part, by the National Science Foundation, United States, and the Electric Power Research Institute, United States. The authors are grateful for this support.

Appendix A. Mesh independence study

To confirm that the CFD simulation results are accurate, a mesh independence study was conducted for the different computational domains including the EVAPCO fins and the manifold fins. A combination mesh including tetrahedral dominant cells, surface topology mapping cells, and finer cell sizes at the wall boundaries was implemented to accurately resolve the heat transfer and pressure drop in the computational domain. Because multiple computational domains were generated in this study based on the fin parameters, every domain was verified separately before finalizing the results. Here we will discuss results for two of the cases investigated in this study, one with the EVAPCO *x1* fins (p = 3 mm) and other with the straight manifold *x1* fins (p = 3 mm). For the EVAPCO *x1* fins, Fig. A1(a) shows the mesh sizes tested for a case of inlet velocity of 6 m/s, and Fig. A1(b) shows the pressure change with the mesh size. Results show that for the highest velocity case tested here, the pressure has reached asymptotic value and therefore, the results are mesh independent. The computational domain for the manifold heat sinks is a little bit more involved, and the mesh independence for this domain is shown in Fig. A2(a)-(d). Fig. A2(a) shows the result for a velocity contour moving along the manifold to explain how the flow moves across the manifold channel from the inlet to the exit. Fig. A2(b) shows the mesh sizes tested for a case of inlet velocity of 6 m/s in the manifold heat sink. As seen in Fig. A2(c), an important difference that was observed in the velocity results was the development of flow “dead” zones in the coarse mesh which showed that the flow was not continuous and may not be converged. On the other hand, the fine mesh showed a continuous flow through the manifold fins. Fig. A2(d) shows the pressure change with the mesh size for the three mesh sizes tested on the manifold. Results show that for the highest velocity case tested here, the pressure has reached asymptotic value and therefore, the results are mesh independent. For all the results discussed in this study, the finest mesh that showed asymptotic values for pressure drop was selected for calculating the final parameters.

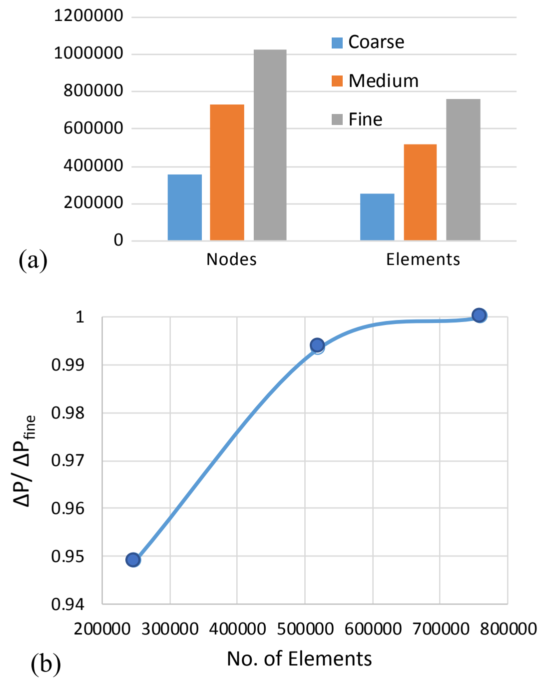

Fig. A1. (a) Mesh sizes used for the computational domain for EVAPCO fins. (b) Pressure drop predictions with mesh size.

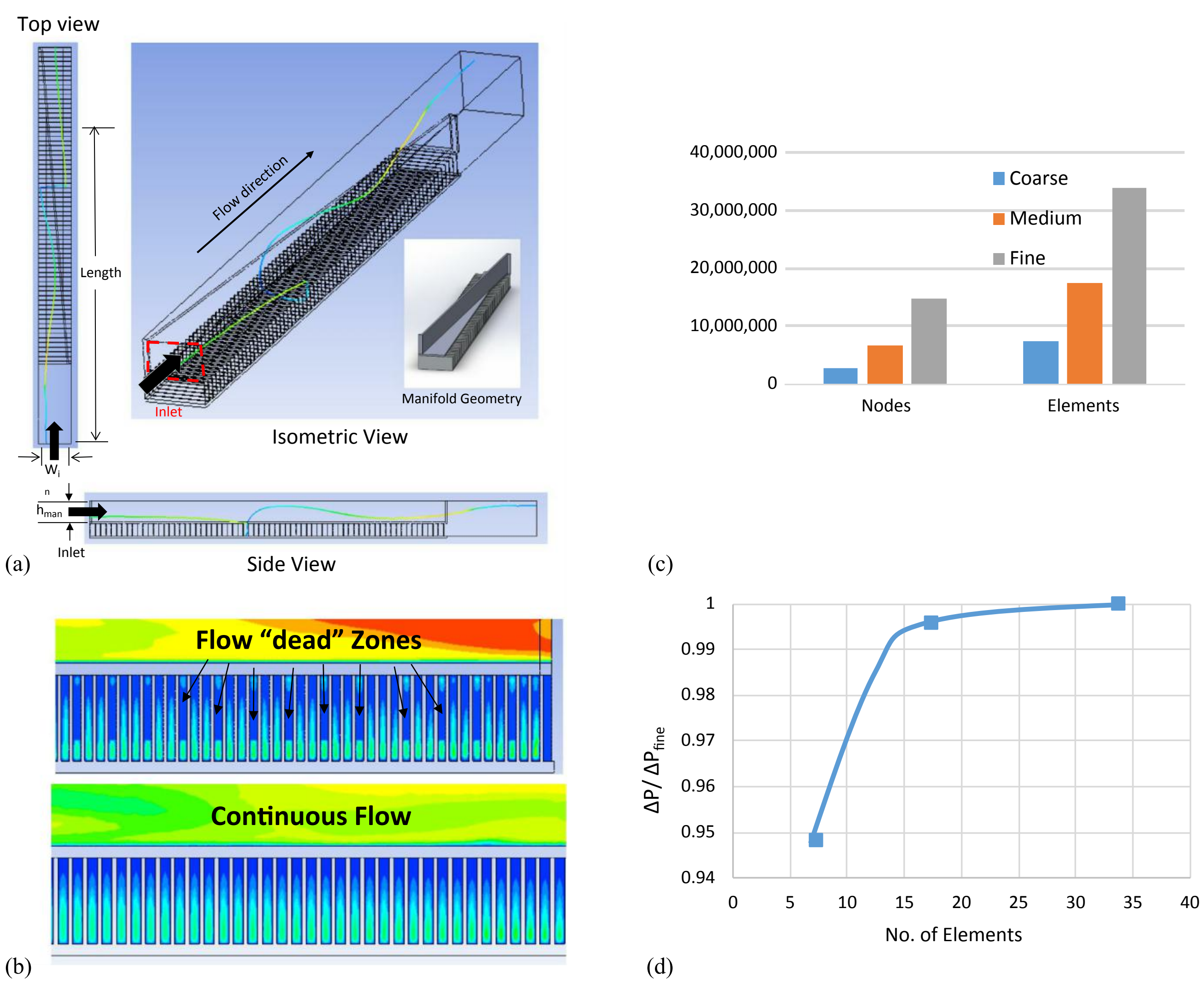

Fig. A2. (a) Two views showing a velocity streamline moving along the 3D manifold channel. (b) Velocity contours showing dead zone predictions for coarse mesh simulations. (C) Mesh sizes for the 3D manifold domain tested in this study, (d) Pressure drop predictions with mesh size.

Appendix B. Supplementary material

Supplementary data to this article can be found online at https://doi.org/10.1016/j.applthermaleng.2019.114700.

References

[1] J.F. Kenny, N.L. Barber, S.S. Hutson, K.S. Linsey, J.K. Lovelace, M.A. Maupin, Estimated use of water in the United States in 2005, US Geological Survey (2009).
[2] A.E. Conradie, D.G. Kröger, Performance evaluation of dry-cooling systems for power plant applications, Appl. Therm. Eng. 16 (1996) 219–232.
[3] EVAPCO-BLCT Brochure, in: EVAPCO, Inc., Westminster, MD, 2017.
[4] K. Zammit, Air-Cooled Condenser Design, Specification, and Operation Guidelines, Tech. rep., Electric Power Research Institute, 2005.
[5] D.G. Kröger, Air-cooled Heat Exchangers and Cooling Towers, PennWell Books, 2004.
[6] J.G. Bustamante, A.S. Rattner, S. Garimella, Achieving near-water-cooled power plant performance with air-cooled condensers, Appl. Therm. Eng. 105 (2016) 362–371.
[7] C.J. Meyer, Numerical investigation of the effect of inlet flow distortions on forced draught air-cooled heat exchanger performance, Appl. Therm. Eng. 25 (2005) 1634–1649, https://doi.org/10.1016/j.applthermaleng.2004.11.012.
[8] P.J. Hotchkiss, C.J. Meyer, T.W. Von Backström, Numerical investigation into the effect of cross-flow on the performance of axial flow fans in forced draught air-cooled heat exchangers, Appl. Therm. Eng. 26 (2006) 200–208.
[9] J.R. Bredell, D.G. Kröger, G.D. Thiart, Numerical investigation of fan performance in a forced draft air-cooled steam condenser, Appl. Therm. Eng. 26 (2006) 846–852.
[10] P. Liu, H. Duan, W. Zhao, Numerical investigation of hot air recirculation of air-cooled condensers at a large power plant, Appl. Therm. Eng. 29 (2009) 1927–1934.
[11] X. Zhang, H. Chen, Effects of windbreak mesh on thermo-flow characteristics of air-cooled steam condenser under windy conditions, Appl. Therm. Eng. 85 (2015) 21–32.
[12] H.T. Liao, L.J. Yang, X.Z. Du, Y.P. Yang, Triangularly arranged heat exchanger bundles to restrain wind effects on natural draft dry cooling system, Appl. Therm. Eng. 99 (2016) 313–324.
[13] Y. Lu, Z. Guan, H. Gurgenci, A. Alkhedhair, S. He, Experimental investigation into the positive effects of a tri-blade-like windbreak wall on small size natural draft dry cooling towers, Appl. Therm. Eng. 105 (2016) 1000–1012.
[14] Y. Kong, W. Wang, X. Huang, L. Yang, X. Du, Y. Yang, Circularly arranged air-cooled condensers to restrain adverse wind effects, Appl. Therm. Eng. 124 (2017) 202–223, https://doi.org/10.1016/j.applthermaleng.2017.06.001.
[15] Y. Kong, W. Wang, X. Huang, L. Yang, X. Du, Y. Yang, Wind leading to improve cooling performance of natural draft air-cooled condenser, Appl. Therm. Eng. 136 (2018) 63–83.
[16] Q. Liu, L. Xia, M. Hu, X. Li, Z. Mi, J. Jia, Positive impact of a tower inlet cover on natural draft dry cooling towers under crosswind conditions, Appl. Therm. Eng. 139 (2018) 283–294, https://doi.org/10.1016/j.applthermaleng.2018.04.129.
[17] M. Goodarzi, R. Ramezanpour, Alternative geometry for cylindrical natural draft cooling tower with higher cooling efficiency under crosswind condition, Energy Convers. Manag. 77 (2014) 243–249, https://doi.org/10.1016/j.enconman.2013.09.022.
[18] Y. Kong, W. Wang, Z. Zuo, L. Yang, X. Du, Y. Yang, Combined air-cooled condenser layout with in line configured finned tube bundles to improve cooling performance, Appl. Therm. Eng. 154 (2019) 505–518, https://doi.org/10.1016/j.applthermaleng.2019.03.099.
[19] A. Dewan, P. Mahanta, K.S. Raju, P.S. Kumar, Review of passive heat transfer augmentation techniques, Proc. Inst. Mech. Eng. Part A J. Power Energy. 218 (2004) 509–527.
[20] J. He, L. Liu, A.M. Jacobi, Air-side heat-transfer enhancement by a new winglet-type vortex generator array in a plain-fin round-tube heat exchanger, J. Heat Transf. 132 (2010) 71801.
[21] H.A. El-Sheikh, S.V. Gurimella, Enhancement of air jet impingement heat transfer using pin-fin heat sinks, IEEE Trans. Compon. Packag. Technol. 23 (2000) 300–308, https://doi.org/10.1109/6144.846768.
[22] C. Hilbert, S. Sommerfeldt, O. Gupta, D.J. Herrell, High performance micro-channel air cooling, in: Semicond. Therm. Temp. Meas. Symp. 1990. SEMI-THERM VI, Proceedings., Sixth Annu. IEEE, IEEE, 1990, pp. 108–113.
[23] S. Laohalertdecha, P. Naphon, S. Wongwises, A review of electrohydrodynamic enhancement of heat transfer, Renew. Sustain. Energy Rev. 11 (2007) 858–876, https://doi.org/10.1016/j.rser.2005.07.002.
[24] M. Legay, N. Gondrexon, S. Le Person, P. Boldo, A. Bontemps, Enhancement of heat transfer by ultrasound: review and recent advances, Int. J. Chem. Eng. 2011 (2011).
[25] A. Bejan, M.R. Errera, Deterministic tree networks for fluid flow: geometry for minimal flow resistance between a volume and one point, Fractals 5 (1997) 685–695.
[26] S.M. Senn, D. Poulikakos, Laminar mixing, heat transfer and pressure drop in tree-like microchannel nets and their application for thermal management in polymer electrolyte fuel cells, J. Power Sources 130 (2004) 178–191.
[27] W. Escher, B. Michel, D. Poulikakos, Efficiency of optimized bifurcating tree-like and parallel microchannel networks in the cooling of electronics, Int. J. Heat Mass Transf. 52 (2009) 1421–1430.
[28] T. Baummer, E. Cetegen, M. Ohadi, S. Dessiatoun, Force-fed evaporation and condensation utilizing advanced micro-structured surfaces and micro-channels, Microelectron. J. 39 (2008) 975–980.
[29] M. Ohadi, K. Choo, S. Dessiatoun, E. Cetegen, Next Generation Microchannel Heat Exchangers, Springer, 2013.
[30] M.A. Arie, A.H. Shooshtari, M.M. Ohadi, Experimental characterization of an additively manufactured heat exchanger for dry cooling of power plants, Appl. Therm. Eng. 129 (2018) 187–198.
[31] R.K. Shah, A.L. London, Laminar Flow Forced Convection in Ducts: A Source Book for Compact Heat Exchanger Analytical Data, Academic press, 2014.
[32] K.W. Jung, C.R. Kharangate, H. Lee, J. Palko, F. Zhou, M. Asheghi, E.M. Dede, K.E. Goodson, Microchannel cooling strategies for high heat flux (1 kW/cm2) power electronic applications, in: Proc. 16th Intersoc. Conf. Therm. Thermomechanical Phenom. Electron. Syst. ITherm 2017, 2017. doi: 10.1109/ITHERM.2017.7992457.